

Clark University

Clark Digital Commons

Geography

Faculty Works by Department and/or School

2003

Measuring the physical composition of urban morphology using multiple endmember spectral mixture models

Tarek Rashed

San Diego State University

John R. Weeks

San Diego State University

Dar Roberts

University of California, Santa Barbara

John Rogan

San Diego State University, jrogan@clarku.edu

Rebecca Powell

University of California, Santa Barbara

Follow this and additional works at: https://commons.clarku.edu/faculty_geography



Part of the [Geography Commons](#)

Repository Citation

Rashed, Tarek; Weeks, John R.; Roberts, Dar; Rogan, John; and Powell, Rebecca, "Measuring the physical composition of urban morphology using multiple endmember spectral mixture models" (2003).

Geography. 686.

https://commons.clarku.edu/faculty_geography/686

This Article is brought to you for free and open access by the Faculty Works by Department and/or School at Clark Digital Commons. It has been accepted for inclusion in Geography by an authorized administrator of Clark Digital Commons. For more information, please contact larobinson@clarku.edu, cstebbins@clarku.edu.

Measuring the Physical Composition of Urban Morphology Using Multiple Endmember Spectral Mixture Models

Tarek Rashed, John R. Weeks, Dar Roberts, John Rogan, and Rebecca Powell

Abstract

The application of multiple endmember spectral mixture analysis (MESMA) to map the physical composition of urban morphology using Landsat Thematic Mapper (TM) data is evaluated and tested. MESMA models mixed pixels as linear combinations of pure spectra, called endmembers, while allowing the types and number of endmembers to vary on a per-pixel basis. A total of 63 two-, three-, and four-endmember models were applied to a Landsat TM image for Los Angeles County, and a smaller subset of these models was chosen based on fraction and root-mean-squared error (RMSE) criteria. From this subset, an optimal model was selected for each pixel based on optimization for maximum area coverage. The resultant endmember fractions were then mapped into four main components of urban land cover: Vegetation, Impervious surfaces, Soil, and Water/Shade. The mapped fractions were validated using aerial photos. The results showed that a majority of the image could be modeled successfully with two- or three-endmember models. The validation results indicated the robustness of MESMA for deriving spatially continuous variables quantified at the sub-pixel level. These parameters can be readily integrated into a wide range of applications and models concerned with physical, economic, and/or socio-demographic phenomena that influence the morphological patterns of the city.

Introduction

A recurrent theme in urban remote sensing studies has been how to derive summary indicators of physical components of urban morphology from remotely sensed data (Green, 1955; Forster, 1985; Ridd, 1995; Jensen and Cowen, 1999). This type of analysis has traditionally been limited due to the spectral heterogeneity of urban features in relation to the spatial resolution of the remote sensing sensors (Weber, 1994). This is especially true in the context of multispectral images with medium spatial resolution such as those provided by Landsat, SPOT, and the Indian satellites. Because of the presence of spectral mixing in the pixels of these images, the identification of urban land cover using per-pixel analytical techniques becomes very difficult because the continuum of land cover cannot be readily divided into discrete classes.

Strahler *et al.* (1986) divide scene models into two types, H- and L-resolution models, depending on the relationship between the size of elements (e.g., vegetation) in the scene and the resolution cell of the sensor. In the H-resolution model, scene elements are larger than resolution cells and, therefore, the spatial arrangement of scene elements can directly be detected. The L-resolution model is the opposite, where scene elements are not individually detectable because they are smaller than the resolution cells. Detecting the spatial arrangement of objects may require a resolution cell size several times smaller than their size. Accordingly, for multispectral images with medium spatial resolution, the scene model of urban landscapes can be regarded as an L-resolution model. Further, as the size of objects in the urban scene becomes increasingly small relative to the resolution cell size, it may no longer be possible to consider objects individually (Strahler *et al.*, 1986). Instead, the urban scene model can be regarded as a continuous model, in which the measurement of each pixel can be treated as a sum of spectral interactions between various scene elements weighted by their concentration or relative aerial proportions within the resolution cell (i.e., a mixture model). Therefore, it can be asserted that, in the context of medium resolution multispectral images, H-resolution models in urban areas should operate in a subservient role to L-resolution models (Graetz, 1990; Rashed *et al.*, 2001; Phinn *et al.*, 2002).

Over the past ten years, there has been a trend toward describing the spatially varying character of land cover in terms of continuous surfaces (Mather, 1999). Through this trend, the proportions of different components of land cover are estimated for each pixel of the image. Fuzzy classification and spectral mixture analysis (SMA) are two groups of techniques that have been proposed to provide *soft* analysis of mixed pixels. The work we present in this paper is based on the SMA approach. The SMA approach assumes that a landscape is formed from continuously varying proportions of idealized types of land cover with pure spectra, called endmembers (Adams *et al.*, 1986; Adams *et al.*, 1993). Endmembers are abstractions of land-cover materials with uniform properties present in the scene. In an urban environment, these may include impervious surfaces, vegetation types, water bodies, and bare soils (Ridd, 1995). Linear SMA is the process of solving for endmember fractions, assuming that the spectrum measured for each pixel represents a linear combination of

T. Rashed, J.R. Weeks, and J. Rogan are with the Department of Geography, San Diego State University, San Diego, CA 92182 (TRashed@mail.sdsu.edu; john.weeks@sdsu.edu; rogan@rohan.sdsu.edu).

D. Roberts and R. Powell are with the Department of Geography, University of California Santa Barbara, Santa Barbara, CA 93106 (dar@geog.ucsb.edu; becky@geog.ucsb.edu).

Photogrammetric Engineering & Remote Sensing
Vol. 69, No. 9, September 2003, pp. 1011–1020.

0099-1112/03/6909-1011\$3.00/0

© 2003 American Society for Photogrammetry
and Remote Sensing

endmember spectra that corresponds to the physical mixture of surface components weighted by their areal abundance. Although nonlinear mixing can be important for some types of analysis, the effects of multiple scattering in the majority of SMA applications are assumed to be negligible (Roberts *et al.*, 1998a; Mather, 1999).

Many SMA applications have been applied to multispectral imagery in non-urban environments (e.g., Roberts *et al.*, 1998b; Rogan *et al.*, 2002), but some recent studies have indicated the feasibility of this technique in urban environments (e.g., Ward *et al.*, 2000; Madhavan *et al.*, 2001; Rashed *et al.*, 2001; Small, 2001; Phinn *et al.*, 2002; Wu and Murray, 2003). Findings from these studies indicate that a classification of the urban scene based on SMA-derived measures may be superior to other traditional per-pixel classifications techniques. However, they also show a higher degree of RMS error associated with these models (Ward *et al.*, 2000; Rashed *et al.*, 2001; Small, 2001). This is because the standard SMA model implements an invariable set of endmembers to model the spectra in all the pixels within an image. The assumption fails to account for the fact that, due to the diversity of urban materials, the number and type of components within the field of view are variable. For example, the endmembers required to describe the central business district of a city are different than those required to describe single family residential districts or urban recreational areas. In addition, if a pixel is modeled by fewer endmembers than required, the unmodeled portion of the pixel spectrum will be partitioned into the resultant fractions, thus increasing the model error for that pixel (Roberts *et al.*, 1998b). Similarly, the use of too many endmembers to unmix the pixel spectrum will result in fraction errors, caused by spectral confusion between these endmembers.

The purpose of this paper is to explore and test the applicability of an algorithm utilizing the technique of multiple endmember spectral mixture analysis (MESMA) (Roberts *et al.*, 1998b) to measure the physical composition of urban morphology from a Landsat TM image. The MESMA approach allows the number and type of endmembers to vary for each pixel in an image. This permits a larger number of endmembers to be modeled within a scene, while meeting the constraints concerning the relationship between the number of image bands and the maximum number of endmembers that

can be modeled in each pixel. Our specific objectives in this paper are

- to demonstrate how MESMA can be utilized to derive comparable physical measures that describe the morphological characteristics of urban areas; and
- to assess the utility of MESMA in the context of an urban environment by (1) comparing the performance of MESMA with that of a standard SMA model, (2) validating endmember fractions produced by MESMA models, and (3) showing examples of how estimated endmember fractions could be related to patterns of urban morphology by applying a model of urban material composition developed by Ridd (1995).

Study Site

This study was undertaken in Los Angeles County, one of the most ethnically diverse places in the United States (Gordon and Richardson, 1999), with a total population exceeding 9.5 million according to data from the 2000 Census. The location of the study area is shown in Figure 1. It represents the metropolitan urbanized region within Los Angeles County, which covers approximately 3220 square kilometers, almost half of the county's total area.

The segregation patterns of ethnicity and socioeconomic classes in Los Angeles, accompanied by successive waves of economic restructuring and population expansion, have been reflected by the built environment and the physical structure of urban form within the region (Allen and Turner, 1997). Li (1998), comparing areas in Los Angeles dominated by population groups from China and Indochina versus those dominated by groups from Taiwan and Hong Kong, showed that even the micro-divisions within the same ethnicity have their geographical expression in the spatial differentiation of urban landscape. Mullens and Senger (1969), using color-infrared (CIR) aerial photos, revealed a highly consistent relationship between the physical surrogates derived from these photos (e.g., vegetation appearance, vacant land, lot and home sizes, pools and patios, street conditions) and the demographic and socioeconomic characteristics of urban neighborhoods in Los Angeles. Herold *et al.* (2002) observed that roof materials in California cities are particularly diverse in material and color, and that this diversity is likely to be influenced by the surrounding land use and neighborhood socioeconomic

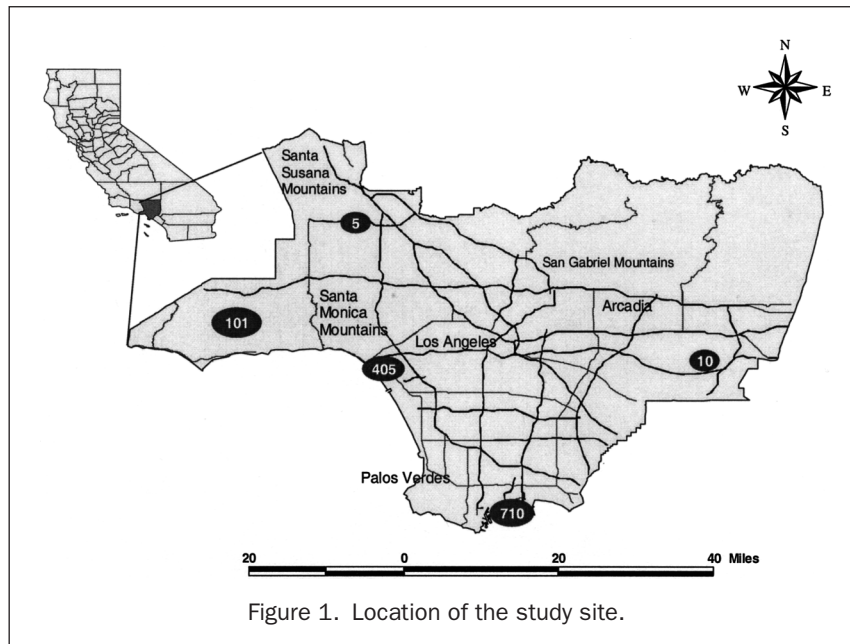
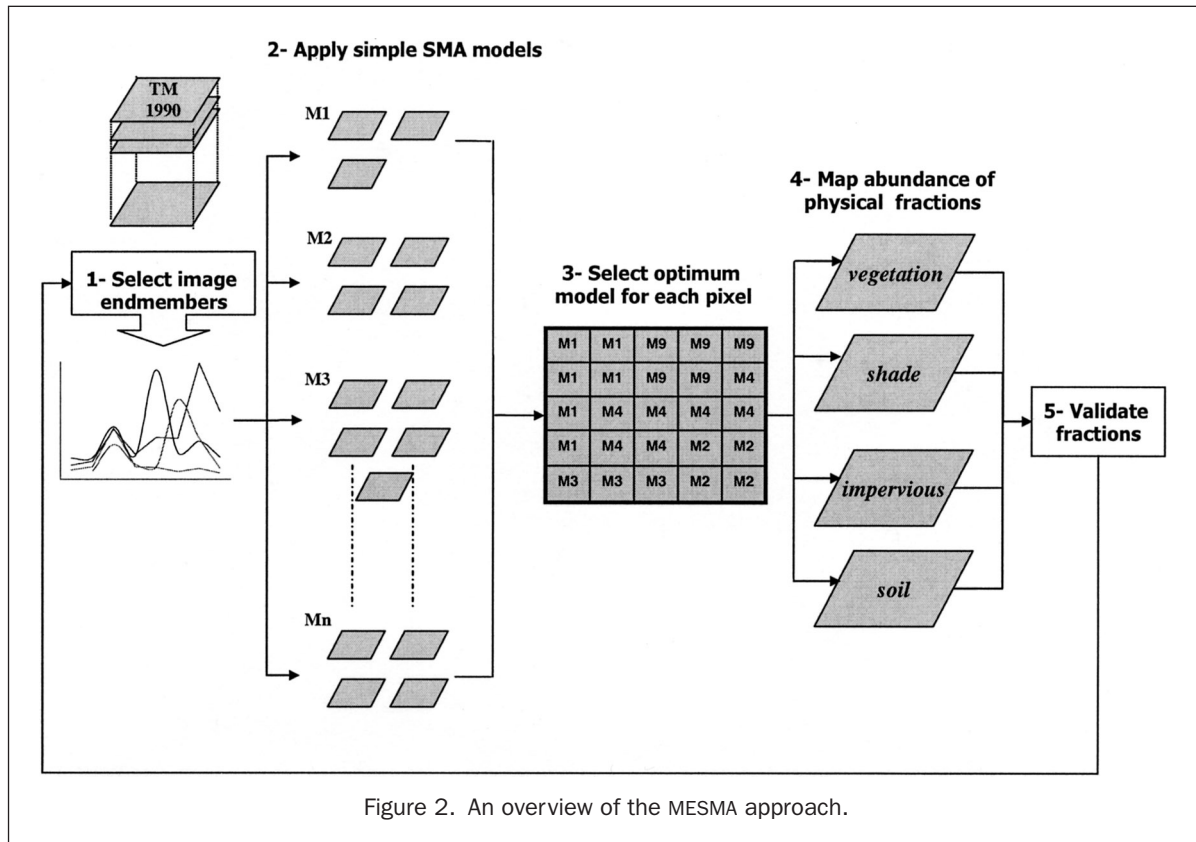


Figure 1. Location of the study site.



characteristics. Miller and Winer (1984) reported differences in vegetation species composition in Los Angeles, not only between residential and non-residential areas (e.g., commercial, industrial), but also between residential areas with different racial profiles.

Therefore, the diverse social and physical character of Los Angeles makes it an ideal study site for testing the capability of MESMA for deriving rigorous measures of urban material compositions from remote sensing imagery. The temporal and spatially explicit characteristics of these measures can then be utilized to examine the degree to which variation in the physical settings is connected to variability in societal attributes. This can help improve our understanding of urban morphological patterns in that region, and ultimately can aid in the formation of policy in anticipation of the problems that accompany urbanization processes and demographic shifts in that region.

Data and Methods

Data

The data utilized in our application of MESMA included a subset (3113 lines by 4801 samples) from a Landsat TM image acquired on 03 September 1990 (path 41, row 36). The acquisition date of this image corresponds reasonably well to the 1990 U.S. Census (taken in April of that year). In addition to the multispectral image, we utilized a set of 1.0-m spatial resolution aerial photos to aid in the validation of the resultant endmember fractions. These photos were generated from 1:12,000-scale color photographs acquired in late 1993 by I.K. Curtis Services, Inc., from an altitude of 2740 m using an RC10 aerial survey camera.

Overview of the MESMA Approach

The MESMA approach, originally developed by Roberts *et al.* (1998b), is based on the concept that, although the spectra in

any individual pixel can be modeled with relatively few endmembers, the number and type of endmembers are variable across an image. In this sense, MESMA can be described as a modified linear SMA approach in which many simple SMA models are first calculated for each pixel in the image. The objective is then to choose, for every pixel in the image, which model among the candidate models provides the best fit to the pixel spectra while producing physically reasonable fractions.

The procedure we followed in applying MESMA to the study area is summarized in Figure 2. As shown in the figure, we started this multistage process by selecting a set of candidate endmembers believed to represent a relatively pure spectral response of the target materials in the scene. In the next step, we applied a series of standard SMA models based on a variety of possible combinations of the endmembers, such that the number of endmembers in any single model is not less than two and not more than the total number of image bands. The performance of all models at each pixel was evaluated to select the smallest subset of candidate models for every pixel in the image. A reliable candidate model is one that produces physically realistic fractions (i.e., between 0 percent and 100 percent) and does not exceed a certain threshold of error. We then ran an optimization program to select an optimal model from the subset of candidate models previously selected for each pixel. Finally, we utilized the fraction values produced by these optimal models to map the abundance of general land-cover components in the urban scene and validated the results using the aerial photos. The procedure is described in more detail below.

Selection of Endmembers

The selection of endmembers can be performed in two ways (Adams *et al.*, 1993): by deriving them (1) directly from the image (image endmembers) or (2) from field or laboratory spectra of known materials (reference endmembers) (see Roberts *et al.* (1998b) for a comparison between the two).

Because of the coarse spectral resolution of the TM image, and because the present analysis uses a single-date image, we deemed it more feasible to use image endmembers. Image endmembers have the advantage of being collected at the same scale as the image and are thus easier to associate with features in the scene.

To select scene elements that represent general categories of land cover, we followed the conceptual model proposed by Ridd (1995). Ridd suggested that various subdivisions of urban areas may be described in terms of proportions of Vegetation (V), Impervious surfaces (I), and Soil (S). Ridd's VIS model offers an intuitively appealing link to the spectral mixing problem because the spectral contribution of its three main land-cover components can be resolved at the sub-pixel level using the SMA technique. The model was originally applied to American cities, but it has also been tested with data from Australia (Ward *et al.*, 2000), Thailand (Madhavan *et al.*, 2001), and Egypt (Rashed *et al.*, 2001). The results of these studies show that the model is robust in describing the urban landscape, although it may be necessary to include an additional component of water or shade to achieve an accurate characterization of urban morphology (Rashed *et al.*, 2001).

The process of image endmember selection commenced by applying the Pixel Purity Index (PPI) method, developed by Boardman *et al.* (1995) to initially screen all the pixels in the image in terms of their relative purity. The PPI method allocates to each pixel in the image a score based on the number of times it is found to occupy a near-vertex position in the repeated projections of the n -dimensional data onto a randomly oriented vector passing through the mean of a data cloud. The resulting score allows reliable identification of image endmembers because those pixels that possess relatively pure spectra will have a high score (i.e., will be found repeatedly at the extremes of the data distribution). Out of the 14,011,347 pixels included in the image, only 2,536 pixels (about 0.018 percent) were identified as "extremes," with PPI scores ranging from 1 to 73 (Figure 3a). Only pixels with a PPI score above the average were then selected as endmember candidates, resulting in a reduction of the total number of extreme pixels to 821. This reduced set of pixels was then divided into smaller subsets based on their clustering in the n -dimension space. These subsets were chosen according to a modified VIS model that also incorporates water or shade as a fourth endmember. A threshold of 50 pixels or more per group of clusters was then used to remove dispersed pixels from the selection, and eight main groups of extreme pixels were identified. Finally, the eight groups of extreme pixels were linked to the image to determine their physical correspondence in the urban scene (with the aid of aerial photos), and the mean spectrum of each group was used as a candidate endmember for unmixing. The spectral profiles of the final set of candidate endmembers are shown in Figure 3b. These included:

- One endmember, Shd (cluster 1), for the water (the ocean, lakes) and shade category.
- Two endmembers, Veg1 and Veg2 (clusters 2 and 3, respectively), for the green vegetation category. Veg1 corresponded to urban vegetation found in residential lawns, gardens, parks, golf courses, cemeteries, and shrublands, while Veg2 was used for natural vegetation located in the coastal sage and chaparral occupying the lower elevations of the Santa Monica and San Gabriel mountains, in addition to the oak-grass woodland located in the eastern portion of the image. The slight difference between the spectral profiles of these two vegetation endmembers is due to the level of liquid water content in natural green vegetation (Veg2) that is higher than that of urban vegetation (Veg1).
- Three endmembers, Imp1, Imp2, and Imp3 (clusters 4, 5, and 6, respectively), for the impervious surface category. While the spectral profiles of these first two endmembers follow the same trend, as indicated in Figure 3b, the brightness values

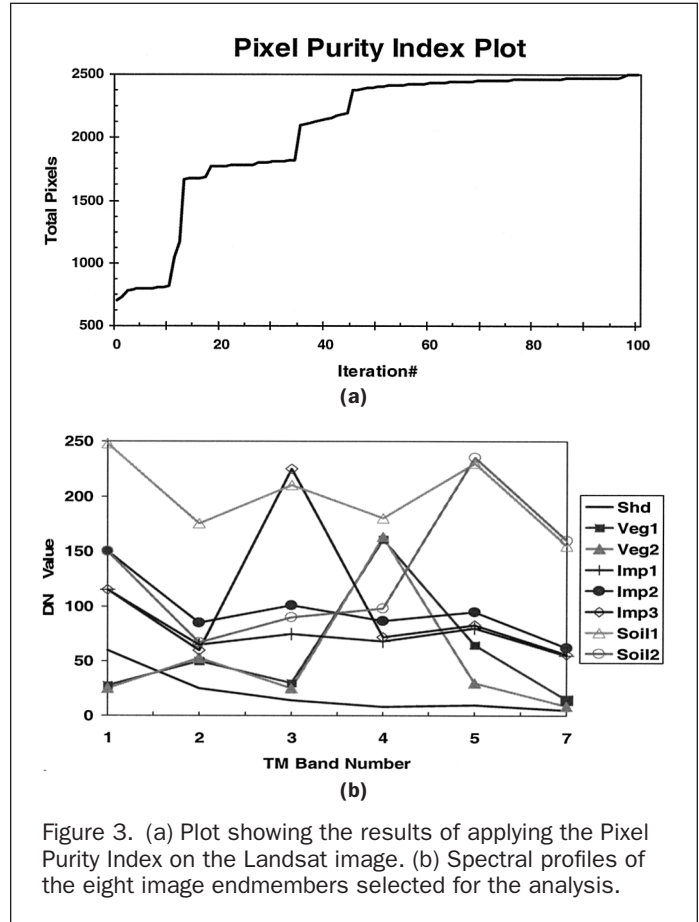


Figure 3. (a) Plot showing the results of applying the Pixel Purity Index on the Landsat image. (b) Spectral profiles of the eight image endmembers selected for the analysis.

vary due to differences in the targets they corresponded to in the urban scene. Imp1 was used as an endmember for parking lots and dark gray roads, whereas Imp2 was used for gray asphalt roofs, red-gray roofs, and light asphalt roads. The Imp3 endmember has a rather distinct spectral profile because it corresponded to red tile roofs and wood shingle roofs.

- Two endmembers, Soil1 and Soil2 (clusters 7 and 8, respectively), for the soil category. The former corresponded to bare soil in the urban scene, while the latter corresponded to sparsely vegetated soils. Observed differences in the spectral profiles of these two endmembers is a result of the variations in the organic matter and mineral compounds between these two soil endmembers.

Generation of SMA Models

Based on the selected set of candidate endmembers, a series of SMA models were identified to model the image scene based on different possible combinations between these endmembers. Given the size of the image, and to minimize the computational time of this process, we restricted the combination of endmembers to only be between the general categories of land cover. For example, the two endmembers Veg1 and Veg2 were not allowed to be used together in any individual model because they belonged to the same vegetation category. This rule resulted in a total of 63 separate mixture models for each pixel in the Landsat scene. These models included 23 two-endmember models, 28 three-endmember models, and 12 four-endmember models. For each one of these 63 candidate models, we employed an algorithm for spectral unmixing that was based on the unconstrained modified Gram-Schmidt least-squares method (Roberts *et al.*, 1998a), in which fractions are constrained to sum to 1 while individual fractions are allowed to be less than 0 or greater than 1. When this method is applied to an image consisting of N spectral bands

using a number of endmembers less than or equal to N , the output will be a fraction image for each endmember and an RMSE image that measures the model's fit. The specific formulation can be found in Adams *et al.* (1993), Tompkins *et al.* (1997), and Roberts *et al.* (1998a).

Optimization of Model Selection

The purpose of this stage of the analysis was to identify, from the 63 models produced in the previous stage, the optimal model for each pixel in the image. A model had the potential to be optimal for a pixel if it minimized the RMSE while providing reasonable (positive and physically meaningful) fractions for that pixel. Because it was possible that more than one model could meet these criteria for a pixel, the selection of optimal models was conducted in two steps. In the first step, a subset of potential candidate models was selected for each pixel according to the following criteria:

- A fraction criterion: A model was considered to be a candidate for a pixel if it produced physically reasonable fractions between -0.05 and 1.05 for that pixel. A 5 percent error in the modeled fractions was permitted to allow for noise-generated errors.
- An RMSE criterion: A model was selected if the RMSE was below a threshold of 0.05 .

Based on these two criteria, an algorithm was developed to screen the fractions and the RMSE results produced by the 63 models in every pixel in the image. The output of this process was an image consisting of 63 bands, each corresponding to one of the 63 models. In each band, if a model met the two criteria for a pixel, that pixel was assigned a value of 1. Otherwise it was assigned a value of 0.

In the second step, the resulting binary fractional bands were further processed by an optimization program to address the case when two or more models have met the criteria in a pixel (i.e., model overlap). In this case, it becomes necessary to choose which model, among these candidates, is optimal for the pixel. We applied an optimization program based on the classical maximal covering problem originally introduced by Church and ReVelle (1974). The objective of this optimization program was to select a final subset of optimal models (one per pixel) that minimizes model overlap while maximizing the number of pixels being correctly modeled in the image. This helped identify the dominant set of models that were more likely to have physical correspondence to the scene than would other spatially fragmented models. The problem formulation of this optimization program is described in detail in Roberts *et al.* (1998b). The program was written to run on the GRID module of the Arc/Info GIS software package.

Validating Fractions

In the final stage of our application of MESMA, the per-pixel optimal models were used to map the fractional abundance of the general components of land cover in the urban scene (i.e., Veg1 and Veg2 endmember fractions were mapped to a vegetation land-cover class, while Soil1 and Soil2 fractions were mapped to a soil land-cover class, and so on). The end product of this process consisted of four maps depicting the spatially varying character of the following land-cover components: Vegetation, Impervious surface, Soil, and Water/Shade. In addition, a map of RMSE was generated showing pixels of higher RMSE (>0.05 DN) which could not be modeled by any of the 63 models.

To assess the accuracy of final fraction maps and to evaluate the robustness of MESMA in the context of the urban environment, aerial photos were utilized to validate the final results. Despite the growing number of studies on SMA, assessing the accuracy of derived endmember fractions through direct quantitative methods is a topic that has been remark-

ably neglected, with the exception of small number of studies that have attempted to address this issue, including Small (2001), Peddle *et al.* (1999), and Elmore *et al.* (2000). The difficulty arises from the fact that natural surfaces composed of a single uniform material do not exist in the real world. Even with human-made materials, factors such as material ageing, atmospheric influences, and other human-related activities have a profound impact on the heterogeneity of urban surfaces. This makes it very difficult to find sufficient reference data that can directly be compared against the continuously varying surface of endmember fractions generated over large areas. The alternative solutions are either to compare the agreement of derived endmember fractions with estimates of fractions derived independently by another method, or to assess the validity of derived fractions in light of their usefulness in providing accurate land-use/land-cover categorical classification of urban areas. Clearly, the former is difficult to pursue because none of the currently competing methods has been proven superior, while the latter defies the objective of our research, which is to describe the continuous nature of the urban landscape.

Acknowledging these limitations, we followed a simple approach to validate endmember fractions through aerial photos by building upon a procedure described in Peddle *et al.* (1999). In this approach, a stratified adaptive cluster sampling (SACS) method was used to identify a number of test sites on the aerial photos. This method was designed to adaptively increase sampling efforts of observed values that satisfy a condition of interest (Thompson, 1992). Our interest here was to find "relatively" homogeneous surfaces that were occupied by endmembers that belonged to one, and only one, of our four categories of land cover. This was achieved by applying a threshold of 0.7 , or greater, to fraction images to delineate all pixels in each image that include at least 70 percent of a single endmember. The threshold of 70 percent was arbitrarily chosen, assuming that when a pixel meets this condition for a certain fractional value, then it is most likely that this pixel can be classified under that "crisp" land-cover class. The spatial clusters of delineated pixels corresponded to urban features that were expected to be homogeneous (e.g., park, an airport runway, parking lot, lake, etc). From this population of spatially clustered pixels, a random subset of test sites was selected and identified on the aerial photos. The boundaries of these test sites were digitized on the aerial photos, and areas of the digitized polygons were then calculated to represent the reference data. For each polygon, the percentage of corresponding endmember fractions in the pixels was summed up to indicate the area of the polygon estimated by MESMA. The accuracy of each endmember fraction (δ) was identified as the mean of the percentage absolute difference between actual and modeled cover estimates, calculated according to the following equation (Peddle *et al.*, 1999):

$$\delta = \sum \frac{|\gamma - \sigma|}{\gamma} / n \quad (1)$$

where γ is the area of a test site, σ is the area calculated by accumulating endmember fractions for that site, and n is the number of test sites identified for each endmember. A total of 16 test sites (four for each land-cover component) were used in the validation process.

Results and Discussion

Evaluation of SMA Models Performance

The performance of the 63 SMA models was evaluated in terms of a model's ability to produce lower RMSE values (<0.05 DN) and physically reasonable fractions for the largest number of pixels. Table 1 lists these 63 models, the

TABLE 1. THE 63 TWO-, THREE-, AND FOUR-ENDMEMBER MODELS USED IN THE ANALYSIS

Two-Endmember Models			Three-Endmember Models			Four-Endmember Models		
Model#	Endmembers	Pixels Modeled	Model#	Endmembers	Pixels Modeled	Model#	Endmembers	Pixels Modeled
1	Shd, Veg1	1 692 347	24	Shd, Veg1, Imp1	3 318 195	52	Shd, Veg1, Imp1, Soil1	11 594 957
2	Shd, Veg2	1 095 685	25	Shd, Veg1, Imp2	4 115 168	53	Shd, Veg1, Imp2, Soil1	7 836 608
3	Shd, Imp1	780 773	26	Shd, Veg1, Imp3	2 171 710	54	Shd, Veg1, Imp3, Soil1	10 538 917
4	Shd, Imp2	860 357	27	Shd, Veg1, Soil1	5 732 480	55	Shd, Veg1, Imp1, Soil2	724 983
5	Shd, Imp3	642 062	28	Shd, Veg1, Soil2	6 502 150	56	Shd, Veg1, Imp2, Soil2	3 083 792
6	Shd, Soil1	1 228 036	29	Shd, Veg2, Imp1	1 964 924	57	Shd, Veg1, Imp3, Soil2	2 716 161
7	Shd, Soil2	3 275 691	30	Shd, Veg2, Imp2	3 074 462	58	Shd, Veg2, Imp1, Soil1	11 538 398
8	Veg1, Imp1	2 061 850	31	Shd, Veg2, Imp3	1 393 240	59	Shd, Veg2, Imp2, Soil1	8 209 641
9	Veg1, Imp2	5 106 606	32	Shd, Veg2, Soil1	6 006 944	60	Shd, Veg2, Imp3, Soil1	10 607 065
10	Veg1, Imp3	5834	33	Shd, Veg2, Soil2	5 07 126	61	Shd, Veg2, Imp1, Soil2	517 036
11	Veg1, Soil1	12 493	34	Shd, Imp1, Soil1	4 800 338	62	Shd, Veg2, Imp2, Soil2	2 461 663
12	Veg1, Soil2	155 703	35	Shd, Imp1, Soil2	426 120	63	Shd, Veg2, Imp3, Soil2	1 877 092
13	Veg2, Imp1	1 278 423	36	Shd, Imp2, Soil1	1 929 781			
14	Veg2, Imp2	4 224 485	37	Shd, Imp2, Soil2	1 476 696			
15	Veg2, Imp3	2708	38	Shd, Imp3, Soil1	1 158 487			
16	Veg2, Soil1	23 193	39	Shd, Imp3, Soil2	1 529 938			
17	Veg2, Soil2	87 669	40	Veg1, Imp1, Soil1	9 824 236			
18	Imp1, Soil1	3 484 584	41	Veg1, Imp1, Soil2	1 593 546			
19	Imp1, Soil2	357 485	42	Veg1, Imp2, Soil1	9 806 578			
20	Imp2, Soil1	2 797 658	43	Veg1, Imp2, Soil2	4 311 990			
21	Imp2, Soil2	1 334 251	44	Veg1, Imp3, Soil1	27 034			
22	Imp3, Soil1	3136	45	Veg1, Imp3, Soil2	72 771			
23	Imp3, Soil2	3514	46	Veg2, Imp1, Soil1	9 571 234			
			47	Veg2, Imp1, Soil2	1 153 540			
			48	Veg2, Imp2, Soil1	10 112 890			
			49	Veg2, Imp2, Soil2	3 923 361			
			50	Veg2, Imp3, Soil1	41 959			
			51	Veg2, Imp3, Soil2	35 734			

endmembers they used, and the actual number of modeled pixels resulting from each one. A comparison between these models is shown in Figure 4 in terms of the percentage of modeled pixels. In this figure, the performance of individual two-endmember, three-endmember, and four-endmember models is shown in Figures 4a, 4b, and 4c, respectively, while Figure 4d shows performance results of the models when they are combined based on the number of endmembers used in the model. These results demonstrate that no single set of endmembers can adequately describe the spectra measured by every pixel in the image. However, the more endmembers that are added to a single model, the better will be the performance of that model. For example, no more than 36 percent of the image was modeled by any one of the 23 two-endmember models. At the same time, several individual three- and four-endmember models accounted for more than 70 percent of land cover in the image. Nevertheless, an increase in the number of endmembers also leads to an increase in the overlap between the models (that is, if a pixel is correctly modeled by two or more SMA models), resulting in similar performance for the combined two-, three-, and four-endmember models after optimization (75 percent, 91 percent, and 86 percent, respectively—Figure 4d).

The effect of model overlap is also illustrated in the decline in the performance between the combined three-endmember models and the combined four-endmember models. This suggests that there is a tradeoff between the number of endmembers utilized in the models and the amount of overlap between the models. Ideally, a better characterization of the urban scene would be achieved when the overlap between models is kept to a minimum so that each model represents spatially contiguous, potentially meaningful features across the urban landscape. This also suggests that the lower RMSE values obtained by the models that utilized four end-member fractions were not due to an accurate utilization of

endmembers, but rather, from the statistical fact that the RMSE value is guaranteed to decrease whenever a new variable is added to a regression model. Hence, the optimum model for a pixel is the one that can correctly model that pixel with a minimum number of endmembers because in this case these endmembers will likely be physically, rather than statistically, meaningful.

Our evaluation of model performance (not shown) suggests that a strategy for selecting those optimal models that better characterize the urban scene is to minimize the model overlap whenever possible. This can be achieved by starting with two-endmember models, evaluating these models in terms of the RSME and fraction criteria, selecting the models that meet these criteria with minor overlap, and then, if necessary, appending additional models that incorporate more endmembers. By adopting this strategy in the optimization program, optimal models were assigned to 98.86 percent of the pixels in the image. The remaining portion of the image (1.14 percent) represented areas with a higher RMSE that could not be adequately modeled by any of the models. The majority of these areas existed in the Santa Susanna Mountains, located in the northwest quadrant of the image.

Analysis of Endmember Fractions

Based on the optimal model selected for each pixel, the abundance of endmember fractions was mapped into the four main categories of the modified VIS model: vegetation, impervious surface, soil, and water/shade. The maps of these generalized fractions are shown in Figure 5. Brighter areas indicate higher fractional abundance of the endmember category while darker areas indicate lower abundance. These fractions provide a measure of the physical properties of the dominant land-cover categories in the scene, thus helping to reveal the physical composition of the morphological patterns of the Los Angeles metropolitan area at the time of image acquisition. For example,

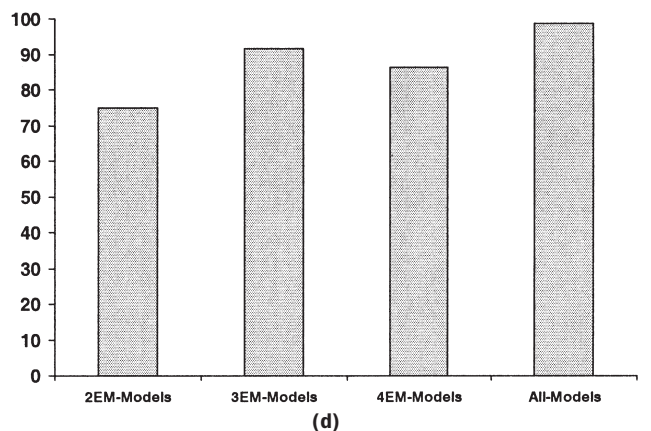
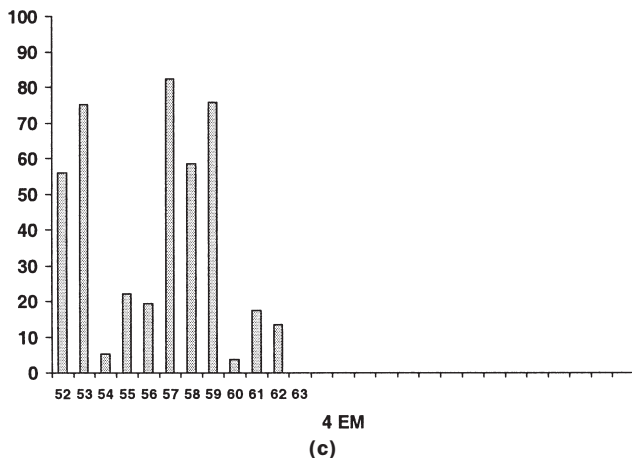
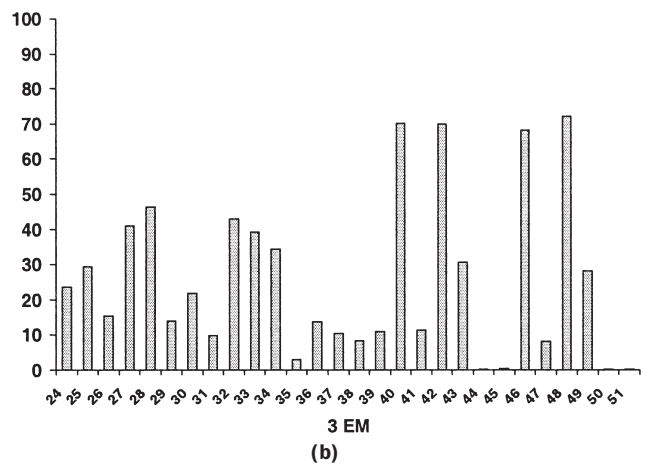
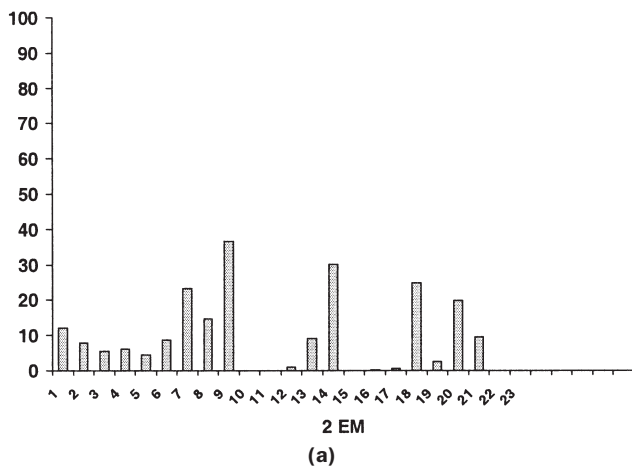


Figure 4. Performance of individual models assessed in terms of the percentage of pixels that met the RMSE and fraction criteria. The results for individual two-, three-, and four-endmember models are shown in (a), (b), and (c), respectively. (d) compares the performance of the models aggregated according to the number of endmembers to the performance of all models combined together. Results shown in (d) were optimized for maximum area coverage.

the spatial distribution of fractions generally resembles the classic concentric model of land use. Fractions of impervious surface are very high in the central business district (CBD) at the urban core (Figure 5b). Moving outward in all directions from the CBD, the proportion of impervious surface decreases. Conversely, vegetation and soil fractions (Figures 5a and 5c) increase as one goes outward from the core to the periphery. Whether vegetation or soil fractions become dominant depends on the ambient environment. Vegetation dominates the northeast and southwest quadrants of the scene where the San Gabriel and the Santa Monica Mountains are located, respectively. Soil dominates the northwest quadrant of the image near the Santa Susanna Mountains and in the southeast quadrant where some industrial areas are located. Although shade fractions are highly sensitive to such factors as topographic effects and solar zenith angle at the time of image acquisition, they are still capable of providing us with a reasonable assessment of features in the scene (Figure 5d). Besides water bodies (e.g., the ocean, lakes), differences in shade abundance can be observed between the CBD with its skyscrapers and other residential areas, between multi-family housing in and around the urban-core and single-family housing on the periphery, and between the different aspects of slope in the mountainous regions.

In this study, our primary objective was to derive measures that can be linked in subsequent research with social variables to describe urban morphological patterns in Los Angeles. It is, therefore, worthwhile to highlight here some indications about the potential linkage between variation in socioeconomic and demographic variables, and the physical variables as determined by the endmember fractions. The network of freeways in Los Angeles acts as a framework for the distribution of endmember fractions, and also for linking variation in these fractions to patterns of ethnicity and socioeconomic segregation in the study area. For example, the non-Hispanic white population is dominant in neighborhoods that extend along the periphery, which score high on the socioeconomic scale. These areas are characterized as having relatively high values of vegetation fraction, given a larger share of private green space (e.g., golf courses, home lawns), medium in impervious surface fractions, and low in shade and soil fractions. The majority of African-American dominated neighborhoods are associated with less affluent areas located in the urban core between the 405 and the 710 freeways. These areas have very low values of vegetation fraction (with the exception of public green spaces such as parks and school yards), high values of shade and impervious surface fractions, and relatively higher soil fractions. This increase in soil fraction

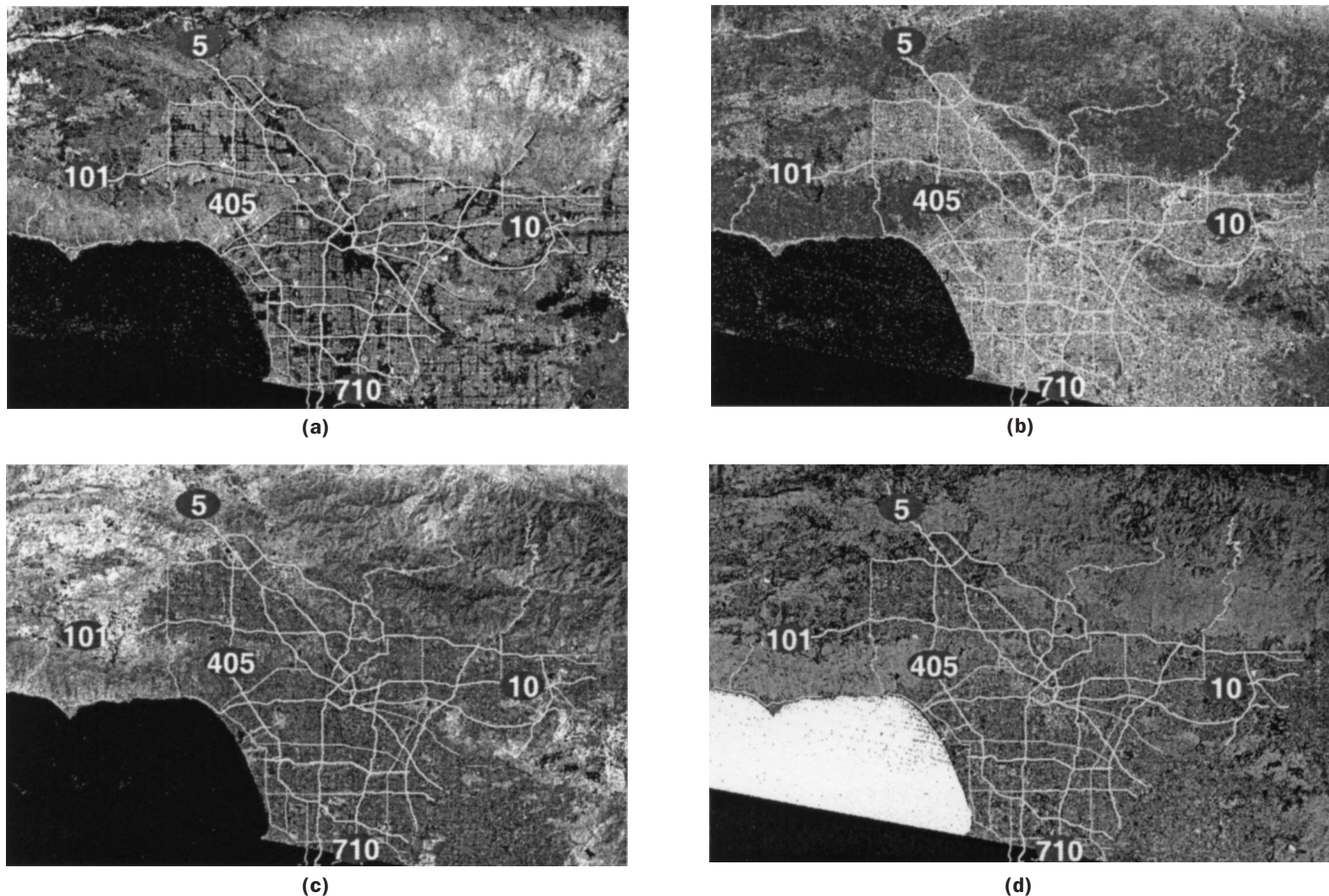


Figure 5. Images produced by mapping endmember fractions from per-pixel optimal models to the four main components of urban land covers: (a) Vegetation, (b) Impervious Surface, (c) Soil, and (d) Water/Shade. Brighter areas indicate higher abundance while darker areas indicate lower abundance.

values indicates a degree of instability associated with reconstruction and development activities that took place in some of these areas in 1990 at the time of image acquisition. Likewise, the Hispanic population is largely concentrated in the central region, which extends along Interstates 10 and 5, to the San Gabriel Valley in the east and the San Fernando Valley in the north. The socioeconomic status of these neighborhoods ranges from low to middle as do the fractions of vegetation, impervious surface, and shade (the latter two are inversely related to the socioeconomic status of the areas).

Fraction Validation Results

The accuracy of MESMA fractions was assessed by comparing the accumulated fraction estimates in relatively homogeneous land-cover components to other estimates derived from the higher resolution aerial photos. We deemed this approach sufficient because, for most applications, one would be interested in the aggregation of fraction measures over well-defined regions (e.g., census tracts, ecological fields), rather than the fractions of an individual pixel. Table 2 shows the results from a comparison of the areal coverage of "reference" homogeneous features obtained from aerial photos, with the area of corresponding features on the image scene calculated through the accumulation of the fractions that were obtained from MESMA. The results indicate that there is good agreement between the measures calculated from the fractions and the aerial-photo-derived estimates for all the four land-cover

components. Both vegetation and soil fractions had the smallest total mean difference from the reference data aggregated over the test sites. The accuracy of impervious surface fractions was slightly lower, while water fractions had the lowest accuracy. These overall accuracy results are also consistent with the individual results by site.

The standard deviation values calculated for each class of land cover provide a complementary measure to assess agreement between reference estimates and MESMA fractions. If MESMA models were consistently overestimating or underestimating the actual areal coverage of a certain class, the distribution of the accumulated fraction estimates for that class would be consistently different from the distribution of the estimates derived from the aerial photos. Therefore, the overall standard deviation values calculated in Table 2 for the four components strengthen the assertion that the distribution of fraction estimates are consistent with the distribution of corresponding aerial-photo-based estimates.

Indeed, we recognize that there is a considerable degree of uncertainty associated with the validation exercise described here. This uncertainty is a product of the flaws and biases resulting from the selection of homogeneous test sites used for the comparison, and from the error associated with the estimation of the areal coverage of these sites from aerial photos. Therefore, the validation exercise described above is obviously incomplete and should be thought of as a first step toward a more strongly quantitative verification of the

TABLE 2. DIFFERENCES BETWEEN ESTIMATES OF MESMA ACCUMULATED FRACTIONS AND AERIAL-PHOTO-DERIVED ESTIMATES. γ AND σ ARE IN SQUARE METERS. δ VALUES ARE CALCULATED ACCORDING TO THE AVERAGE PERCENTAGE OF THE ABSOLUTE DIFFERENCES IN AREAL COVERAGE (NO UNITS), WITH A MAXIMUM POSSIBLE VALUE OF 1

Fraction	Reference γ	Accumulated Fractions σ	$ \gamma - \sigma $	$\frac{ \gamma - \sigma }{\gamma}$	δ	Std
Vegetation						
Site1	242 500	235 181	7318.75	0.031	0.066	0.048
Site2	211 250	244 350	33 100	0.135		
Site3	325 000	336 713	11 712.5	0.035		
Site4	1 034 375	1 104 975	70 600	0.064		
Impervious Surface						
Site1	101 875	102 263	387.5	0.004	0.082	0.065
Site2	1 743 125	1 869 581	126 456.3	0.068		
Site3	25 000	29 813	4812.5	0.161		
Site4	718 750	794 419	75 668.75	0.095		
Soil						
Site1	128 125	138 544	10 418.75	0.075	0.066	0.022
Site2	125 000	132 019	7018.75	0.053		
Site3	302 500	333 225	30 725	0.092		
Site4	1 321 250	1 265 175	56 075	0.044		
Water/Shade						
Site1	310 625	267 525	43 100	0.161	0.145	0.184
Site2	298 125	304 425	6300	0.021		
Site3	279 375	469 631	190 256.3	0.405		
Site4	450 000	455 006	5006.25	0.011		

MESMA-derived fractions. Nevertheless, the preliminary results of this exercise suggest that it is possible to quantify the general land-cover components shaping the physical structure of urban morphology from multispectral images with medium spatial resolution. The results also confirm that MESMA is robust and well suited to provide measures that appropriately describe the physical composition of urban morphology.

Summary and Conclusions

In this paper, we described an approach for measuring the physical composition of urban morphology from medium resolution multispectral satellite images using a multiple end-member spectral mixture analysis (MESMA). The technique has the potential for providing a direct measure of the basic elements that comprise the morphology of the city through a process of pixel-unique endmember selection, based on an optimization technique that minimizes model overlap. We tested this approach in the urban context of Los Angeles County—an area with diverse physical and social settings that are rapidly changing due to a range of complex, interrelated forces of urbanization that are not yet well understood. Using MESMA, we showed that two- and three-endmember models can provide better separation of urban materials than can four-endmember models because of reduced model overlap. We mapped the derived endmember fractions into four general components of urban land cover and demonstrated how these fractions can be linked to the spatial patterns that exist in the region by ethnicity and socioeconomic class.

It has been suggested that urban morphology is “the physical appearance of social reality” (Pesaresi and Bianchin, 2001, p. 56). The potential of MESMA to contribute to urban morphological analysis lies in its ability to quantify the physical composition of urban areas occasioned by human activity at different geographic scales. This serves as an image-derived proxy for human behavior taking place on the ground that we might not otherwise be able to measure. The research presented herein is a work in progress and we recognize that there are limitations in the results. Specifically, we recognize the need to adopt a more rigorous method to validate MESMA

results based on simultaneously acquired, high-resolution hyperspectral imagery with coincident field measurement. However, the aim of this paper is to illustrate the capability of MESMA for providing ways of generating physically meaningful estimates of urban morphology that are not measurable by other means. In future research, we will explore in more detail how these remotely sensed measures can be linked with socio-demographic variables to reveal different morphological patterns of human settlements in large cities.

Acknowledgments

This research has been supported by grants from the National Science Foundation (BCS-0117863 and BCS-0095641). The authors would like to thank the anonymous reviewers for their extremely helpful comments.

References

- Adams, J.B., M.O. Smith, and P.E. Johnston, 1986. Spectral mixture modeling: A new analysis of rock and soil types at the Viking Lander site, *Journal of Geophysical Research*, 91:8098–8112.
- Adams, J.B., M.O. Smith, and A.R. Gillespie, 1993. Imaging spectroscopy: Interpretation based on spectral mixture analysis, *Remote Geochemical Analysis: Elemental and Mineralogical Composition* (C.M. Pieters and P. Englert, editors), Cambridge University Press, Cambridge, United Kingdom, pp. 145–166.
- Allen, J.P., and E. Turner, 1997. *The Ethnic Quilt: Population Diversity in Southern California*, Center for Geographical Studies, California State University, Northridge, California, 282 p.
- Boardman, J.W., F.A. Kruse, and R.O. Green, 1995. Mapping target signatures via partial unmixing of AVIRIS data, *Summaries of the Fifth JPL Airborne Earth Science Workshop*, 23–26 January, Pasadena, California (JPL Publications 95-1, Jet Propulsion Laboratory, Pasadena, California), pp. 23–26.
- Church, R.L., and C.T. ReVelle, 1974. The maximal covering location problem, *Papers of Regional Science Association*, 32:101–118.
- Elmore, A.J., J.F. Mustard, S.J. Manning, and D.B. Lobell, 2000. Quantifying vegetation change in semiarid environments: Precision and accuracy of spectral mixture analysis and the normalized difference vegetation index, *Remote Sensing of Environment*, 73:87–102.

- Forster, B.C., 1985. An examination of some problems and solutions in monitoring urban areas from satellite platforms, *International Journal of Remote Sensing*, 6(1):139–151.
- Gordon, P., and H.W. Richardson, 1999. Review essay: Los Angeles, city of angels? No, city of angles, *Urban Studies*, 3:575–591.
- Graetz, R.D., 1990. Remote sensing of terrestrial ecosystem structure: An ecologist's pragmatic view, *Ecological Studies: Remote Sensing of Biosphere Functioning* (R.J. Hobbs and H.A. Moony, editors), Springer-Verlag, New York, N.Y., pp. 79–85.
- Green, N.E., 1955. *Using Aerial Photography in the Analysis of Urban Structure: Ecological and Social*, Ph.D. dissertation, University of North Carolina, Chapel Hill, North Carolina, 274 p.
- Herold, M., M. Gardner, B. Hadely, and D.A. Roberts, 2002. The spectral dimension in urban land cover mapping from high-resolution optical remote sensing data, *3rd International Symposium: Remote Sensing of Urban Areas*, 11–12 June, Istanbul, Turkey, (Istanbul Technical University), pp. 77–91.
- Jensen, J.R., and D.C. Cowen, 1999. Remote sensing of urban/suburban infrastructure and socio-economic attributes, *Photogrammetric Engineering & Remote Sensing*, 65(5):603–610.
- Li, W., 1998. Anatomy of a new ethnic settlement: The Chinese ethnoburb in Los Angeles, *Urban Studies*, 35(3):479–501.
- Madhavan, B.B., S. Kubo, N. Kurisaki, and T.V.L.N. Sivakumar, 2001. Appraising the anatomy and spatial growth of the Bangkok metropolitan area using a Vegetation-Impervious-Soil model through remote sensing, *International Journal of Remote Sensing*, 22(5):789–806.
- Mather, P.M., 1999. Land cover classification revisited, *Advances in Remote Sensing and GIS Analysis* (P.M. Atkinson and N.J. Tate, editors), John Wiley & Sons Ltd., Chichester, West Sussex, United Kingdom, pp. 7–16.
- Miller, P.R., and A.M. Winer, 1984. Composition and dominance in Los Angeles basin urban vegetation, *Urban Ecology*, 8:29–54.
- Mullens, R.H.J., and L.W. Senger, 1969. *Analysis of Urban Residential Environments Using Color Infrared Aerial Photography: An Examination of Socioeconomic Variable and Physical Characteristics of Selected Areas in the Los Angeles Basin*, Interagency Report from the U.S. Geological Survey to NASA, U.S. Geological Survey, Reston, Virginia, 177 p.
- Peddle, D.R., F.G. Hall, and E.F. LeDrew, 1999. Spectral mixture analysis and geometric-optical reflectance modeling of boreal forest biophysical structure, *Remote Sensing of Environment*, 67:288–297.
- Pesaresi, M., and A. Bianchin, 2001. Recognizing settlement structure using mathematical morphology and image texture, *Remote Sensing and Urban Analysis* (J.-P. Donnay, M.J. Barnsley, and P.A. Longley, editors), Taylor & Francis, London, United Kingdom, pp. 55–67.
- Phinn, S., M. Stanford, P. Scarth, A.T. Murry, and P.T. Shyy, 2002. Monitoring the composition of urban environments based on the Vegetation-Impervious Surface-Soil (VIS) model by subpixel techniques, *International Journal of Remote Sensing*, 23(20): 4131–4153.
- Rashed, T., J. Weeks, M. Gadalla, and A. Hill, 2001. Revealing the anatomy of cities through spectral mixture analysis of multispectral satellite imagery: A case study of the greater Cairo region, Egypt, *Geocarto International*, 16(4):5–16.
- Ridd, M., 1995. Exploring a V-I-S (Vegetation-Impervious Surface-Soil) model for urban ecosystem analysis through remote sensing: Comparative anatomy of cities, *International Journal of Remote Sensing*, 16(12):2165–2185.
- Roberts, D.A., G.T. Batista, J.L.G. Pereira, E.K. Waller, and B.W. Nelson, 1998a. Change identification using multitemporal spectral mixture analysis: Applications in eastern Amazonia, *Remote Sensing Change Detection: Environmental Monitoring Applications and Methods* (R.S. Lunetta and C.D. Elvidge, editors), Ann Arbor Press, Ann Arbor, Michigan, pp. 137–161.
- Roberts, D.A., M. Gardner, R. Church, S. Ustin, G. Scheer, and R.O. Green, 1998b. Mapping chaparral in the Santa Monica Mountains using multiple endmember spectral mixture model, *Remote Sensing of Environment*, 65:267–279.
- Rogan, J., J. Franklin, and D.A. Roberts, 2002. A comparison of methods for monitoring multitemporal vegetation change using Thematic Mapper imagery, *Remote Sensing of Environment*, 80:142–157.
- Small, C., 2001. Estimation of urban vegetation abundance by spectral mixture analysis, *International Journal of Remote Sensing*, 22(7):1305–1334.
- Thompson, S.K., 1992. *Sampling*, John Wiley and Sons Inc., New York, N.Y., 343 p.
- Tompkins, S., J.F. Mustard, C.M. Pieters, and D.W. Forsyth, 1997. Optimization of endmembers for spectral mixture analysis, *Remote Sensing of Environment*, 59:472–489.
- Ward, D., S.R. Phinn, and A.T. Murray, 2000. Monitoring growth in rapidly urbanization areas using remotely sensed data, *The Professional Geographer*, 52(3):371–385.
- Weber, C., 1994. Per-zone classification of urban land cover for urban population estimation, *Environmental Remote Sensing from Regional to Global Scales* (G.M. Foody and P.J. Curran, editors), John Wiley & Sons Ltd., Chichester, United Kingdom, pp. 142–148.
- Wu, C., and A.T. Murray, 2003. Estimating Impervious surface distribution by spectral mixture analysis, *Remote Sensing of Environment*, 84:493–505.